ADVANCED HEALTHCARE MATERIALS
www.advhealthmat.de

Small Intestinal Submucosa Membrane Modified by Fusion Peptide-Mediated Extracellular Vesicles to Promote Tissue Regeneration

Lei Zhang, Shiqing Ma, Pengfei Wei, Yifan Zhao, Yuzhu Mu, Jinzhe Wu, Wei Jing, Bo Zhao, Jiayin Deng,* and Zihao Liu**

Tissue injury, which often occurs in daily life, remains challenging in clinical medicine. Developing a novel biomaterial with the capability to provide an ideal microenvironment and homeostasis around the wound is highly desirable for effective tissue regenerative medicine. The small intestinal submucosa (SIS) membrane possesses a precise spatial structure with excellent biocompatibility. Extracellular vesicles (EVs) derived from umbilical cord mesenchymal stem cells can achieve rapid cell proliferation and migration with little immune response by creating a satisfactory microenvironment. In this study, fusion peptide-mediated EVs are able to modify the surface of the SIS membrane via specific combination. In vitro studies prove that modified SIS membranes can promote cell migration and spreading. This phenomenon may be because of the activation of TEADs, which regulate cell behavior. By constructing a rat abdominal wall defect model, it is further demonstrated that the modified SIS membrane is more conducive to tissue regeneration. Collectively, these results suggest that SIS membranes modified by fusion peptide-mediated EVs achieve excellent biofunction and provide promising prospects for tissue regeneration.

1. Introduction

Tissue damage caused by disease or trauma causes pain, functional defects, and aesthetic and psychological problems in patients. Appropriate treatment promotes cell proliferation and migration by providing an environment conducive to wound healing, thus inducing tissue regeneration.[1] Traditional patch materials, such as polypropylene (PP), polyethylene terephthalate (PET), and polyvinylidene fluoride (PVDF),[2] are prone to cause chronic pain, severe infection, and other complications because they are non-degradable and cannot provide a microenvironment suitable for tissue repair. To our knowledge, the local microenvironment around the wound, which involves cell-to-cell communication, cell-to-extracellular matrix interaction, signaling molecules, oxygen and nutrition, contributes to the course of tissue regeneration.[3] Therefore, a novel biomimetic patch that can not only degrade but also establish a proper local microenvironment for tissue regeneration is urgently needed

The small intestinal submucosa (SIS) membrane is one of the most widely applied extracellular matrix (ECM) materials in the treatment of cardiovascular disease, hernia repair, cervical surgery, tracheal tympanic membrane repair, and other soft tissue damage because of its extensive source and great degradability.[4] The natural composition of collagen and abundant bioactive factors, including transforming growth factor-β (TGF-β), glycoproteins, and fibronectin, provide SIS membrane with a 3D spatial structure for cellular adhesion and spread as well as excellent biocompatibility.[5]

In fact, membrane implantation relies mainly on the pattern of endogenous tissue regeneration to complete continuous and dynamic remodeling, which requires a variety of chemical agents and cytokines.[6] Therefore, the presence of bioactive components in the microenvironment is crucial for this complicated process. Considering that biological patches are exogenous biomaterials, the repair process induced by SIS material is extremely dependent on the cellular state (such as recruitment and differentiation of stem cells) and the potential immunogenicity of the material itself, so the SIS membrane is still insufficient in microenvironment simulation and tissue induction. Therefore, loading more bioactive substances on SIS material is conducive to regenerative wound therapy.

Mesenchymal stem cells (MSCs), as seed cells effectively applied in tissue engineering, can increase cell–cell communication by regulating the expression of cytokines and growth factors.[7] However, intra-arterial injection of MSCs has been shown to lead to myocardial microinfarction in dogs,[8] unveiling the risk of immune rejection and embolism. MSC-derived extracellular

L. Zhang, S. Ma, Y. Zhao, Y. Mu, J. Wu, J. Deng, Z. Liu
School and Hospital of Stomatology
Tianjin Medical University
12 Observatory Road, Tianjin 300000, China
E-mail: jdeng@tmu.edu.cn; liuzihao@tmu.edu.cn
P. Wei, W. Jing, B. Zhao
Beijing Biosis Healing Biological Technology Co., Ltd
No. 6 Plant West, Valley No. 1 Bio-medicine Industry Park, Beijing 102600, China
E-mail: zhaobo@biosishealing.com
The ORCID identification number(s) for the author(s) of this article can be found under https://doi.org/10.1002/adhm.202101298

DOI: 10.1002/adhm.202101298

vesicles (EVs), the paracrine mediators responsible for transmitting signal molecules to surrounding cells,[9] participate in maintaining the stability of the microenvironment by activating the immune response and accelerating the release of harmful substances in cells.[10] In addition, EVs present no risk of tumorigenesis and embolism,[11] making them ideal substitutes for stem cells.

EVs derived from umbilical cord mesenchymal stem cells (ucMSCs) can regulate the cellular immunologic response, revascularization and tissue reconstruction during wound healing.[12] Moreover, exosomal miR-1263 of exosomes derived from ucMSCs directly targets Mob1 in recipient cells to inhibit apoptosis and achieve rapid cell proliferationand finally obtain a better tissue-inductive property.[13] However, traditional loading methods for EVs, such as direct absorption and chemical coating, have disadvantages of low loading efficiency, sudden release in vivo and destruction of EVs' structure,[14] which may affect the therapeutic effect and limit wide application. To overcome these limitations, novel fusion peptides were used to realize the specific adsorption of EVs and facilitate the healing process in our study.

Fusion peptide technology allows independent functional peptides to be linked together to form a novel peptide chain with diverse functions.[15] A previous study reported that enhanced binding affinity to collagen materials and angiogenic activity of hepatocyte growth factor (HGF) were obtained by constructing a fusion protein.[16] Owing to their low molecular weight and low cytotoxicity, fusion peptides are less likely to cause innate immune responses and have high bioavailability.[17] CP05 is a small molecule peptide and can specifically bind to CD63, which is a tetrameric protein typically enriched on the surface of EVs.[18] Considering that the main components of the SIS membrane are type I and type III collagen, two collagen-binding peptides (LHERHLNNN and KELNLVY) that are able to anchor biomolecules on the surface of type I and type III collagen, respectively, were used in this study.[19] Consequently, we designed a series of fusion peptides to achieve specific combination and affinity loading of EVs onto the SIS membrane by connecting LHERHLNNN and KELNLVY with CP05, with or without a flexible linker (GGGGS) (**Figure 1A**). This modification conferred a better tissue regeneration effect on the SIS membrane.

2. Results and Discussion

2.1. Structure and Hydrophilicity Prediction of Peptides

As shown in Figure 1, four peptides composed of different components, CP05 (CRHSQMTVTSRL) and CBP (LHERHLNNN or KELNLVY), with (Pep1, Pep2) or without (Pep3, Pep4) a linker (GGGGS), were investigated. Collagen binding peptides LHERHLNNN and KELNLVY were used in this study because they rely on either nonspecific electrostatic interactions or specific interactions to bind to collagen.[19] Another functional peptide CP05 is responsible for anchoring EVs.[18b] Meanwhile, the flexible linker GGGGS was originally chosen to provide structural flexibility and maintain the distance between two functional domains,[20] consequently enhancing the ability of CP05 to capture EVs. The secondary and 3D structures of Pep1–4 shown in Figure 1 illustrate that the four peptides have different predicted molecular architectures. According to the secondary structure, the fusion peptides had basic structures including α-helices, β-sheets, coils, and turns. The GGGGS section presents a random coil structure and stronger mobility, which may provide CP05 with a wider mobile range. In addition, the flexible linker GGGGS can resist proteases,[21] decreasing the rate of degradation in vivo. The hydrophilicity analysis showed amphipathic structures of Pep1–4, and the hydrophilicity of Pep3 was slightly higher than the hydrophilicity of Pep1, whereas Pep4 was weaker than Pep2, which may be owing to the conformational effects caused by direct connection of two functional peptide domains in Pep4.[22]

2.2. EVs Characterization

EVs were purified from the culture medium of ucMSCs by ultracentrifugation. The morphology observed by transmission electron microscopy (TEM) showed a typical round or cup shape (**Figure 2A**). Particle size analysis revealed that the diameters of the extracted vehicles ranged from ≈50 to 200 nm, and the average particle size of EVs was ≈141.9 ± 1.2 nm (Figure 2B,C), consistent with the TEM results. Some peaks that appeared beyond 200 nm may be caused by the aggregation of EVs or impurities. Moreover, as a main basis of EV identification, western blot analysis demonstrated that the characteristic surface markers CD63, CD9, and Alix were positive and that Cytochrome C was negative (Figure 2D). These results were consistent with a previous study,[18b,c] suggesting that EVs were successfully isolated. To identify the size and morphology of EVs after binding to fusion peptides, TEM and nanoparticle tracking analysis (NTA) were carried out. The results showed that the morphology and particle size of EVs did not change significantly (Figure S1, Supporting Information). The quantitative relationship between fusion peptides and EVs was estimated by standard curve (Figure S2, Supporting Information), which indicated that there were ≈1.26×10^{-14} M fusion peptide on one EV when co-incubated with $Pep_{1\&2}$ and were about 1.13×10^{-14} M fusion peptide when co-incubated with $Pep_{3\&4}$.

2.3. Characterization of Modified SIS Membrane

The concentration screening pre-experiment was carried out. Confocal laser scanning microscopy (CLSM) images (Figure S3, Supporting Information) showed that Pep1–4 could achieve good binding effect with SIS membrane at 200×10^{-6} M.

As shown in **Figure 3A**, the surface morphology of each group was characterized by scanning electron microscopy (SEM) images. The unmodified SIS membrane had an asymmetric structure, including a dense layer and a loose layer. Compared with the SIS group, fine particles could be seen on the surfaces of the SIS-EVs, SIS-$Pep_{1\&2}$-EVs, and SIS-$Pep_{3\&4}$-EVs groups, and the SIS-$Pep_{1\&2}$-EVs group had the largest number of particles. Meanwhile, the modification of the SIS membrane did not change its intrinsic structure.

A group of typical CLSM images revealed the binding of peptide-mediated EVs to the loose layer of SIS membrane (Figure 3B). A previous study reported that the content of type I

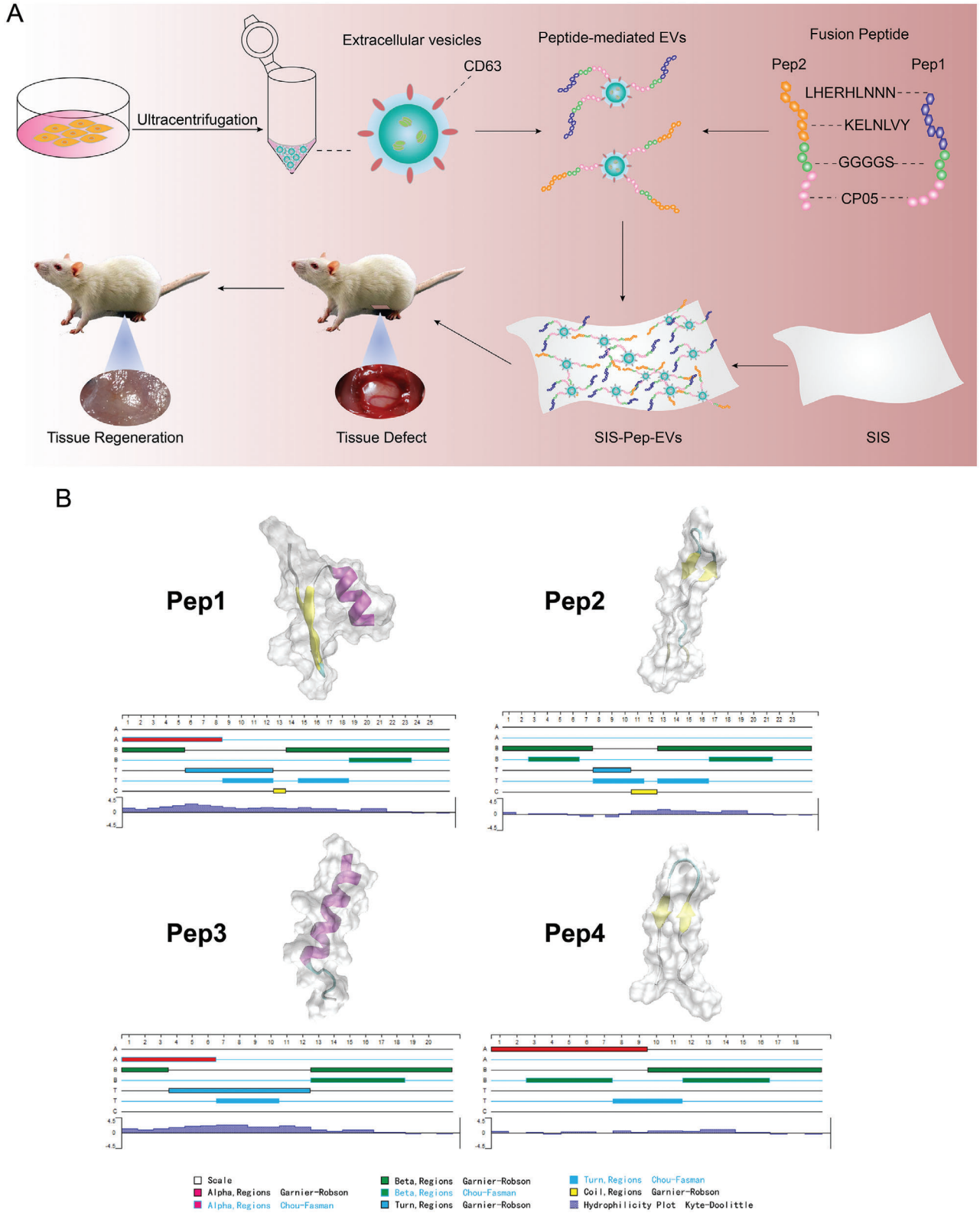

Figure 1. Schematic of the modified SIS membrane and structure prediction of fusion peptides. A) Schematic diagram of the SIS membrane modified by fusion peptide-mediated EVs. LHERHLNNN: type I collagen binding peptide; KELNLVY: type III collagen binding peptide; GGGGS: linker, to connect functional domains; CP05: CRHSQMTVTSRL, to anchor EVs. Fusion peptides without linker were not shown. B) Secondary and 3D structure prediction and analysis of the hydrophilicity of Pep1–4. Pep1: LHERHLNNNGGGGSCRHSQMTVTSRL; Pep2: KELNLVYGGGGSCRHSQMTVTSRL; Pep3: LHERHLNNNCRHSQMTVTSRL; Pep4: KELNLVYCRHSQMTVTSRL. White: coil; purple: α-helix; yellow: β-sheet; cyan: turn.

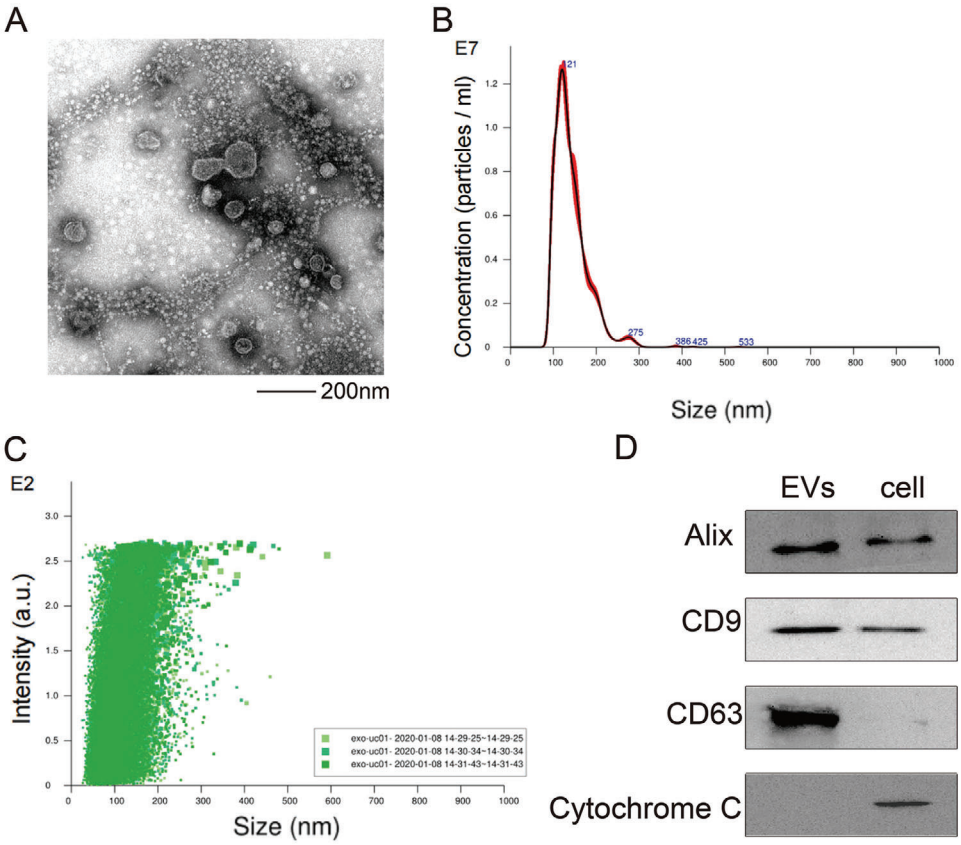

Figure 2. Characterization of EVs. A) Transmission electron microscopy (TEM) image of EVs (20k×). B) Particle size distribution of EVs revealed by Nanosight. C) Intensity and size distribution of EVs. D) Western blot analysis to identify the expression of Alix, CD63, CD9, and Cytochrome C in EVs.

collagen and type III collagen in our SIS membrane was 28.09 ± 0.67% and 59.50 ± 1.42%, respectively.[23] However, CLSM observations showed that there was no significant difference in fluorescence signal intensity between Alexa Fluor 405-labeled type III collagen-binding peptides and fluorescein isothiocyanate (FITC)-labeled type I collagen-binding peptides, which was inconsistent with the ratio of collagen. This phenomenon might be due to the stronger binding ability of LHERHLNNN than KELNLVY. Specifically, particles on the SIS-$Pep_{1\&2}$-EVs group were finer and more homogeneously distributed, demonstrating a better targeting efficiency of the SIS-$Pep_{1\&2}$-EVs group. Moreover, compared with SIS-$Pep_{3\&4}$-EVs, there were more DiI-stained EVs on SIS-$Pep_{1\&2}$-EVs, and the SIS-EVs group showed the fewest fluorescent particles, indicating an effective anchoring phenomenon of $Pep_{1\&2}$. Meanwhile, the loading efficiency increased in the order of SIS-EVs, SIS-$Pep_{3\&4}$-EVs and SIS-$Pep_{1\&2}$-EVs, showing a similar trend with CLSM (Figure S4, Supporting Information). Interestingly, some EVs are co-localized with the fusion peptides, but many EVs are still distributed around the fusion peptides. This may be because of the mechanical displacement of the EVs caused by the binding of fusion peptides to collagen at different sites on SIS membrane. The results of CLSM in the dense layer of modified SIS membranes are similar to those in the loose layer (Figure S5, Supporting Information), which demonstrated that there might be no significant difference in the regeneration effect between dense and loose layers.

The release of fusion peptides and EVs was also observed by CLSM (Figure 3C and Figure S6, Supporting Information). The amino acids Cys and Met are susceptible to oxidation reactions and can be oxidized by oxygen in the air,[24] which affects the stability of peptides. Fusion peptides and EVs on SIS membranes of all groups decreased gradually with time, probably attributed to the degradation and release of these active substances as well as the rupture of collagen fibers to a certain extent. During the whole process, SIS-$Pep_{1\&2}$-EVs showed the most fusion peptides and EVs, indicating a stronger function of $Pep_{1\&2}$. These images indicated that the GGGGS domain might enhance the expression efficiency of collagen-binding peptide and improve biological activity.

Taken together, these results implied that modified SIS membranes were successfully obtained. Researchers have reported that the flexibility of a linker is related to the cooperative function of protein moieties, indicating the importance of linker flexibility in the construction of fusion peptides.[21] More desirable modification effects of Pep1 and Pep2 on the SIS membrane may be ascribed to the existence of GGGGS, which serves as a passive linker to achieve an appropriate separation[25] of collagen-binding peptide and CP05, resulting in a satisfactory bioactivity of the fusion peptide. Therefore, we can assume that the GGGGS used in this study is sufficient to maintain stability and, as a result, provides a suitable structure of the fusion peptide. It will be further discussed in the in vitro experiments whether the fusion

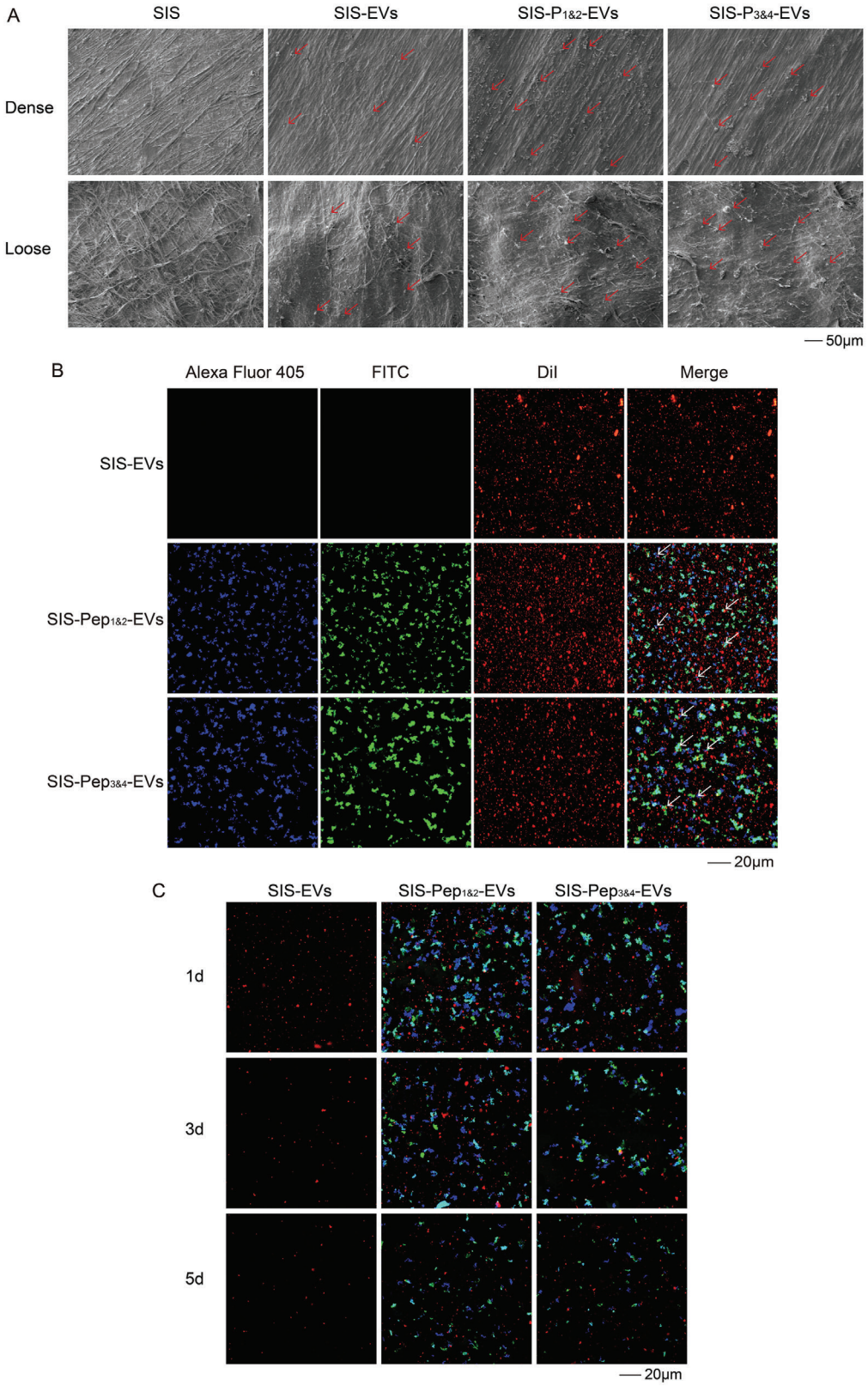

Figure 3. Characterization of SIS, SIS-EVs, SIS-Pep$_{1\&2}$-EVs, and SIS-Pep$_{3\&4}$-EVs membranes. A) SEM images to observe the surface morphology. Red arrows refer to the fusion peptides and EVs (500×). B) CLSM images of loose layer of the SIS-EVs group, SIS-Pep$_{1\&2}$-EVs group, and SIS-Pep$_{3\&4}$-EVs group. Pep1 or Pep3 was labeled with FITC (green), Pep2 or Pep4 with Alexa Fluor 405 (blue), and EVs were labeled with DiI (red). White arrows refer to EVs co-localized with the fusion peptides. C) Release of fusion peptides and EVs after immersion in PBS for 1, 3, and 5 d.

peptide constructed with the collagen-binding peptide and CP05 with GGGGS has a more positive influence on cell behaviors than the fusion peptide constructed with the collagen-binding peptide and CP05 without a linker.

2.4. Biocompatibility Assays and Cell Behaviors

The proliferation and migration of fibroblasts are essential steps in tissue regeneration. Accumulating evidence suggests that uMSC-EVs can regulate the tissue repair course by stimulating cell proliferation and migration.[12b,26] Therefore, CCK-8, Transwell and fluorescence assays were used to explore a series of cell activities in vitro.

To maintain homeostasis, EVs need to be taken up by surrounding cells.[27] **Figure 4A** depicts the uptake of EVs by cells after 12, 24, and 48 h of culture. The results showed that the fluorescence intensity increased over time and reached a peak at 24 h, demonstrating that EVs could be transported to recipient cells to regulate cell behaviors in prophase of tissue regeneration. At 48 h, the fluorescence intensity decreased slightly, which indicated that EVs were metabolized in cells.

The biocompatibility of the modified SIS membrane was assessed by CCK-8 cell counting analysis (Figure 4B). In the case of the SIS-$Pep_{1\&2}$-EVs sample, cells showed the highest proliferative activity after 24 h. Meanwhile, cells in each group proliferated with time and reached the plateau stage at 6 d. The proliferative capability of cells in the SIS-EVs, SIS-$Pep_{1\&2}$-EVs, and SIS-$Pep_{3\&4}$-EVs groups was higher than the proliferative capability of the blank group, indicating that modified SIS membranes were noncytotoxic.

A Transwell trial was carried out to determine the migration ability of NIH3T3 cells incubated with different samples (Figure 4C,D). Quantification of migrated cells is compiled in Figure 4C. In the case of SIS-$Pep_{1\&2}$-EVs and SIS-$Pep_{3\&4}$-EVs, the number of cells passing through the membrane was remarkably higher than the number of cells passing through the membrane in the blank plate, SIS and SIS-EVs groups. This finding illustrates that the modified SIS membrane can elicit rapid migration of cells into soft tissue defects and possibly facilitates tissue regeneration in this way. The SIS-$Pep_{1\&2}$-EVs group was more beneficial to cell motility because more cells in the SIS-$Pep_{1\&2}$-EVs group migrated through the membrane than in the SIS-$Pep_{3\&4}$-EVs group.

The morphology of fibroblasts seeded on SIS, SIS-EVs, SIS-$Pep_{1\&2}$-EVs, and SIS-$Pep_{3\&4}$-EVs was observed by CLSM (Figure 4E). Confocal images showed that fibroblasts adhered to SIS-$Pep_{1\&2}$-EVs and SIS-$Pep_{3\&4}$-EVs for 6 h exhibited a more stellate-patterned phenotype, whereas the fibroblasts adhered to SIS and SIS-EVs membranes were spherical or narrow. After culture for 24 h, cells in the SIS-$Pep_{1\&2}$-EVs and SIS-$Pep_{3\&4}$-EVs groups had well-stretched actin bundles. Especially on SIS-$Pep_{1\&2}$-EVs, cells exhibited better spreading morphology with the largest mean cell area and perimeter (Figure S7, Supporting Information), confirming enhanced cell attachment and cytoskeleton development.

Based on these results, modified SIS membranes possess ideal biocompatibility and noncytotoxicity toward fibroblasts, indicating an important role in cell proliferation, migration, and adhesion because of the ECM-mimetic nanofibrous structure and introduction of EVs. Additionally, SIS membranes modified by peptide-mediated EVs exhibit a stronger ability to promote cell activities, implying that peptide-specifically captured EVs have potential applications in material modification. Apparently, in this study, EVs released from modified SIS membranes in the early stage are helpful to regulate intercellular communication, improve the microenvironment, and finally activate a cascade of cell responses. EVs affect cellular and tissue homeostasis in multicellular organisms via the mechanisms of transducing proteins, lipids, nucleic acids, and other metabolites.[28] Accordingly, in this study, EVs possibly control material-to-cell contacts that influence signal molecule transfer and ultimately the microenvironment, thus modulating the fate of receptor cells. These data also identify better biofunctions of the fusion peptide with the linker GGGGS, which could demonstrate that direct fusion between the collagen-binding peptide and CP05 might cause misfolding and have a little effect on its function.

2.5. Mechanism of Cell Behavior

To investigate the regeneration mechanism of SIS-Pep-EVs, RNA-seq, and clustering analysis were performed to screen the differential gene expression (**Figure 5A**,**B**). Compared with the other groups, the SIS-$Pep_{1\&2}$-EVs group showed enrichment in TEAD transcription factors (TEAD1–4), which are crucial for development, proliferation, tissue homeostasis, and regeneration.[29] Among these factors, TEAD1 was reported to be associated with cell proliferation, migration and survival.[30] Through further exploration, Vgll3, the known transcription coactivator of TEADs, was also found to be increased in the SIS-$Pep_{1\&2}$-EVs group. Other components served as target genes of TEAD, such as CYR61 and BIRC5, which were upregulated in cells of the SIS-$Pep_{1\&2}$-EVs group. Therefore, we used quantitative real-time polymerase chain reaction (qRT-PCR) and western blot to detect the expression of these factors.

CYR61 is a downstream gene of TEAD critical for cell proliferation and migration.[29] BIRC5, also known as survivin, can inhibit cell apoptosis.[31] The qRT-PCR analysis results showed that after 3 d, the SIS-$Pep_{1\&2}$-EVs group had the highest mRNA levels of Vgll3, TEAD1, CYR61, and BIRC5 (Figure 5C). Consistently, western blot analysis showed that the expression of TEAD1, BIRC5, and CYR61 was the highest in the SIS-$Pep_{1\&2}$-EVs group compared with the other groups after 3 d of incubation (Figure 5D,E). Immunofluorescence of CYR61 also showed that the fluorescence intensity of the SIS-$Pep_{1\&2}$-EVs group was stronger than that of the other groups (Figure 5F), indicating an increased expression level.

The Hippo pathway, which plays an important role in organ size regulation, tissue regeneration, and carcinogenesis,[32] has been widely concerned in recent years. The TEAD transcription factor family is an important part of the Hippo pathway. According to above results, Vgll3 and TEAD1 were upregulated in the SIS-$Pep_{1\&2}$-EVs group and then drove the transcription of downstream factors to regulate cell behaviors. Furthermore, the interaction between Vgll3 and TEAD1 is involved in muscle

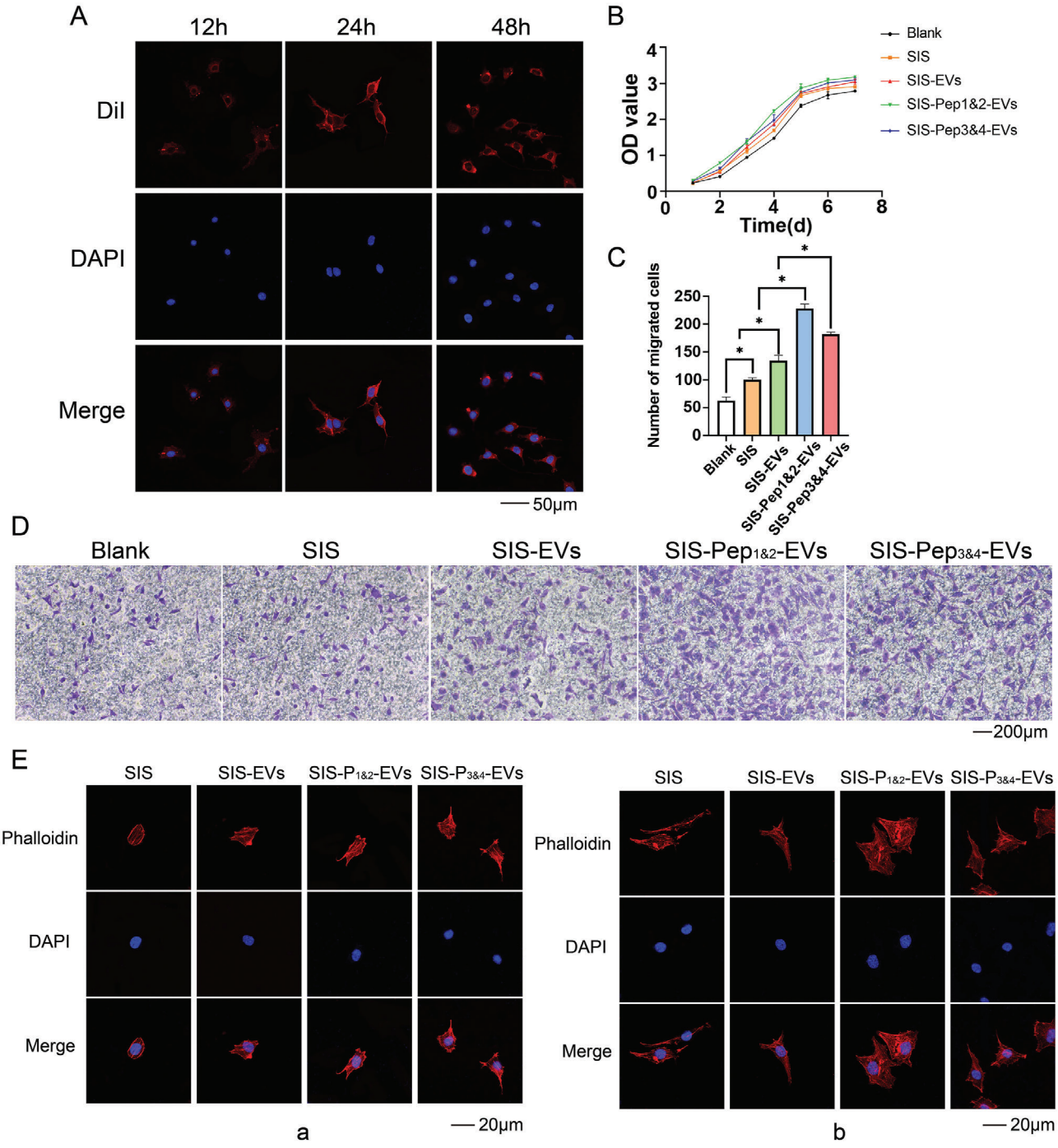

Figure 4. Cell biological behavior and biosafety evaluation of the SIS, SIS-Pep$_{1\&2}$-EVs, and SIS-Pep$_{3\&4}$-EVs groups. A) CLSM of EVs uptake by cells at 12, 24, and 48 h. Blue: DAPI, red: DiI. B) CCK-8 growth curve of NIH3T3 cells seeded on each sample treated after 1, 2, 3, 4, 5, 6, and 7 d of culture. C) Quantitative analysis of cell migration. One-way ANOVA was used for statistical analysis. Data expressed as mean ± SD, $n = 3$, $^*P < 0.05$. D) Transwell images to evaluate the migration of NIH3T3 cells cultured with five groups. E) Fluorescent staining after a) 6 and b) 24 h of cell culture showed the morphological characteristics of cells. Blue: DAPI; red: Rhodamine-conjugated phalloidin.

regeneration.[33] Hence, we postulate that the acceleration of regeneration is due partly to Vgll3 and TEAD1 reactions operating with the Hippo pathway by SIS-Pep$_{1\&2}$-EVs. In addition, several studies have manifested that EVs accelerate cutaneous wound healing by transferring miR-21-3p and that the expression of inflammatory genes is reduced when miR-146a is delivered by exogenous EVs in endotoxin injury models.[34] Hence, we speculate that miRNAs contained in EVs may primarily assist in soft tissue regeneration. Further transcriptome sequencing studies of SIS-Pep$_{1\&2}$-EVs are required.

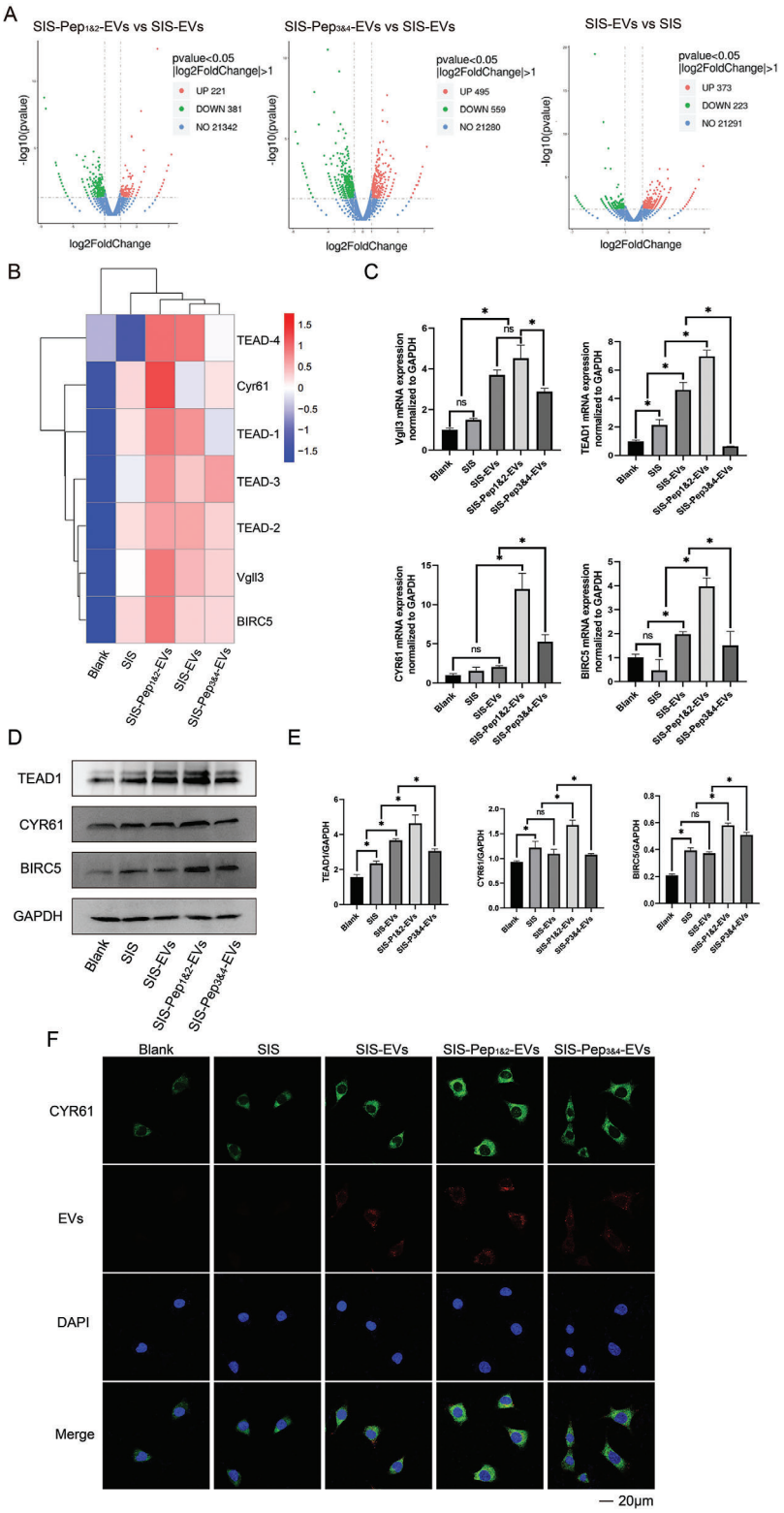

Figure 5. Study on the mechanism of promoting tissue regeneration. A) Differentially expressed genes in each group were screened by RNAseq assay. B) Heat map of cluster analysis of related genes. C) qRT-PCR analysis of Vgll3, TEAD1, CYR61, and BIRC5 expression levels in each group at Day 3. One-way ANOVA was used for statistical analysis. Data expressed as mean ± SD, $n = 3$, $^*P < 0.05$. D) Western blot for TEAD1, CYR61, and BIRC5 in NIH3T3 cells grown on different groups was obtained at Day 3. GAPDH was used as a normalization control. E) Quantitative analysis of western blot analysis. One-way ANOVA was used for statistical analysis. Data expressed as mean ± SD, $n = 3$, $^*P < 0.05$. F) Immunofluorescence image of CYR61. Red: EVs, green: CYR61, blue: DAPI.

2.6. In Vivo Wound Healing Assay

To explore the healing efficiency of the modified SIS membrane on the remodeling process, different samples were applied to an abdominal wall defect model in rats. In vitro experiments showed a better effect of SIS-$Pep_{1\&2}$-EVs on cell proliferation and migration than the effect of SIS-$Pep_{3\&4}$-EVs. Therefore, only SIS-$Pep_{1\&2}$-EVs were applied in the in vivo experiment.

Considering that the fusion peptides used in this study consisted of collagen binding peptide and CP05, in vivo toxicity experiment was conducted to verify whether the modified SIS membrane has any effect on the body. The results showed that there was no significant difference in serum analysis of ALT, AST, BUN, and Crea among the groups (Figure S8, Supporting Information), indicating that the modified SIS membrane was relatively safe without hepatotoxicity and nephrotoxicity.

Morphological observation of the repaired site (Figure S9, Supporting Information) showed that the three groups were not completely healed at 7 d postoperation. The SIS-$Pep_{1\&2}$-EVs group had the smallest defect area, and mild inflammatory reactions could be observed in all groups. At 14 d, obvious connective tissue formation was observed, and the proportion of the defect area decreased gradually. After 30 d, the modified SIS membrane was almost replaced by regenerated tissue without apparent foreign body reaction. In the SIS group, repair of the abdominal wall could also be seen, but the remodeling process was longer than the remodeling process in the SIS-$Pep_{1\&2}$-EVs group.

Hematoxylin and eosin (H&E) staining of tissues in the surgical area was performed to observe SIS membranes and the reaction with the body after implantation (**Figure 6** and Figure S10, Supporting Information). At 7 d, inflammatory cells were found in all groups. Meanwhile, in the SIS-$Pep_{1\&2}$-EVs group, there were fewer inflammatory cells than in the SIS group, and inflammatory cells gradually faded away. At 7 d, all SIS membranes began to biodegrade, and they were covered with more fibrous tissue at 14 d. At 30 d, only a small part of the SIS membrane remained in all groups. Degraded membranes were replaced by regenerative tissue. Thereafter, SIS-$Pep_{1\&2}$-EVs exhibited better biocompatibility because this group presented fewer inflammatory cells in the newly formed tissue, also suggesting that SIS-$Pep_{1\&2}$-EVs may have stronger anti-inflammatory ability, providing a microenvironment in favor of tissue regeneration.

The formation of collagen was observed by Masson's trichrome staining (Figure 6 and Figure S10, Supporting Information). The collagen content in the three groups increased with time, whereas earlier neovascularization and more collagen deposition were observed in the SIS-$Pep_{1\&2}$-EVs group. More collagen with an arrangement similar to normal tissue could be seen in the SIS-$Pep_{1\&2}$-EVs group without tissue fibrosis at 30 d. This phenomenon indicated that SIS-$Pep_{1\&2}$-EVs can reduce the occurrence of complications, mainly the decrease in abdominal wall compliance.[35]

Immunohistochemical analysis was used to assess the expression of related regulatory factors in tissue repair. CD34 was used to detect the density of neovascularization. As shown in **Figure 7** and Figure S10 (Supporting Information), among the three groups, the CD34 expression level was the highest in the SIS-$Pep_{1\&2}$-EVs group and the lowest in the SIS group at 7 and 14 d, suggesting that SIS-$Pep_{1\&2}$-EVs were conducive to the formation of blood vessels. Additionally, the SIS-$Pep_{1\&2}$-EVs group had more TGF-β1-positive cells at 7 and 14 d but fewer TGF-β1-positive cells at 28 d around the defect area. Meanwhile, relatively weak positive expression of TGF-β1 was observed in the SIS group. The expression levels of TGF-β1 and CD34 in the SIS-EVs group were between the expression levels of TGF-β1 and CD34 in the SIS and SIS-$Pep_{1\&2}$-EVs groups. TGF-β1 can regulate inflammatory reactions, angiogenesis, and the synthesis of collagen as well as connective tissue.[36] Nevertheless, extended activity will result in tissue fibrosis and scarring.[37] These results suggested that SIS-$Pep_{1\&2}$-EVs may promote TGF-β1 expression in the initial stage of tissue regeneration and reduce expression in the final stage to prevent fibrosis formation.

In vivo experiments showed a fast rate of SIS membrane degradation. Therefore, more active substances must be introduced to provide a better microenvironment for tissue regeneration. These data showed the validity of the modified SIS membrane and that SIS-$Pep_{1\&2}$-EVs contributed to the early phase of remodeling, which was in accordance with in vitro experiments. An improved microenvironment for the tissue regeneration and healing process was continuously generated by EVs released from SIS-$Pep_{1\&2}$-EVs. In addition, the therapeutic features of EVs are attributed to their immunomodulatory and immunosuppressive activities. EVs have been reported to suppress the concentration of cytokines, including interleukin 1 beta (IL-1β) and tumor necrosis factor alpha (TNF-α), while increasing TGF-β secretion, thereby modulating the immune microenvironment around the wound.[38] Therefore, cross-talk mediated by peptide-mediated EVs between the microenvironment and cells is beneficial to enhance the functional properties of the SIS membrane. Initial healing accelerated by the modified SIS membrane and sustained release of EVs promise to promote tissue reconstruction and restore body function as early as possible.

3. Conclusions

In conclusion, the SIS membrane was treated with EVs mediated by fusion peptides composed of collagen-binding peptide and CP05 in the present study. SIS-$Pep_{1\&2}$-EVs exhibited an enhanced impact on cell proliferation and migration because of EVs released from the modified SIS membrane, resulting in rapid tissue reconstruction of the abdominal wall. This novel membrane is a promising material for tissue regeneration and deserves further research.

4. Experimental Section

Design and Synthesis of Fusion Peptides: Fusion peptides were commercially synthesized (Jill Biochemistry Co., Ltd., Shanghai, China) using the Fmoc (9-fluorenylmethyloxycarbonyl) method. The sequences of the fusion peptides are shown in Table S1 (Supporting Information). The purity of each peptide was at least 95%. The molecular architectures of fusion peptides used in this study were predicted and analyzed by the protein analysis website Robetta. The results were displayed by VMD software. Prediction of hydrophilicity was performed with DNAStar.

Cell Culture: EV-free fetal bovine serum (FBS; Gibco, USA) was obtained by 8 h of centrifugation at 10 000*g*. Rat umbilical cord mesenchymal stem cells (rucMSCs) purchased from Qincheng Biotechnology Co., Ltd. (Shanghai, China) were cultured with Dulbecco's modified Eagle's

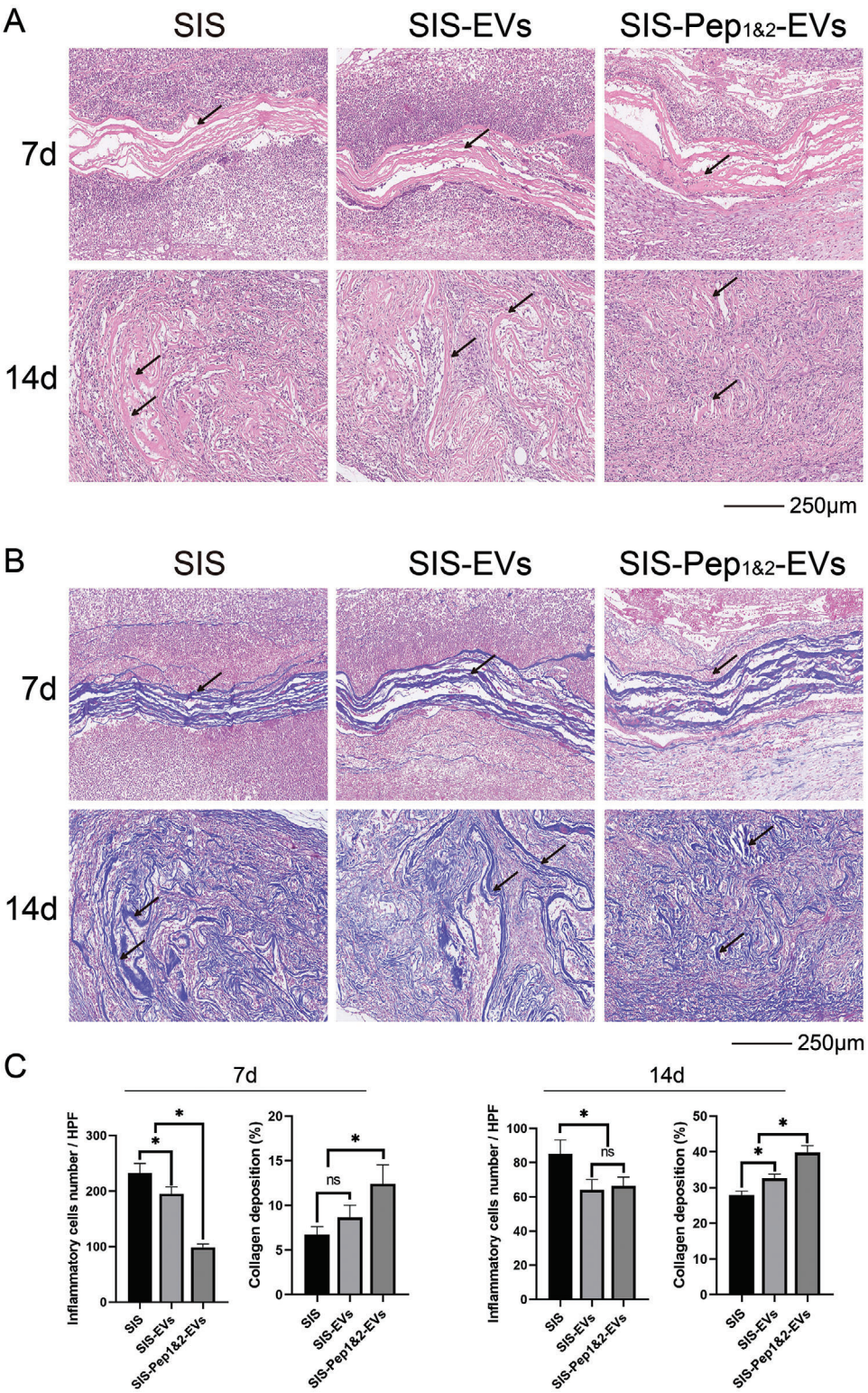

Figure 6. Histological analysis. A) HE staining and B) Masson's trichrome staining of the SIS, SIS-EVs, and SIS-Pep$_{1\&2}$-EVs groups at 7 and 14 d. (SIS membranes were marked by one-way arrows.) C) Inflammatory cells and collagen deposition of different groups. All data were displayed as mean ± SD, $n = 6$, $^*P < 0.05$. One-way ANOVA was used to analyze the results.

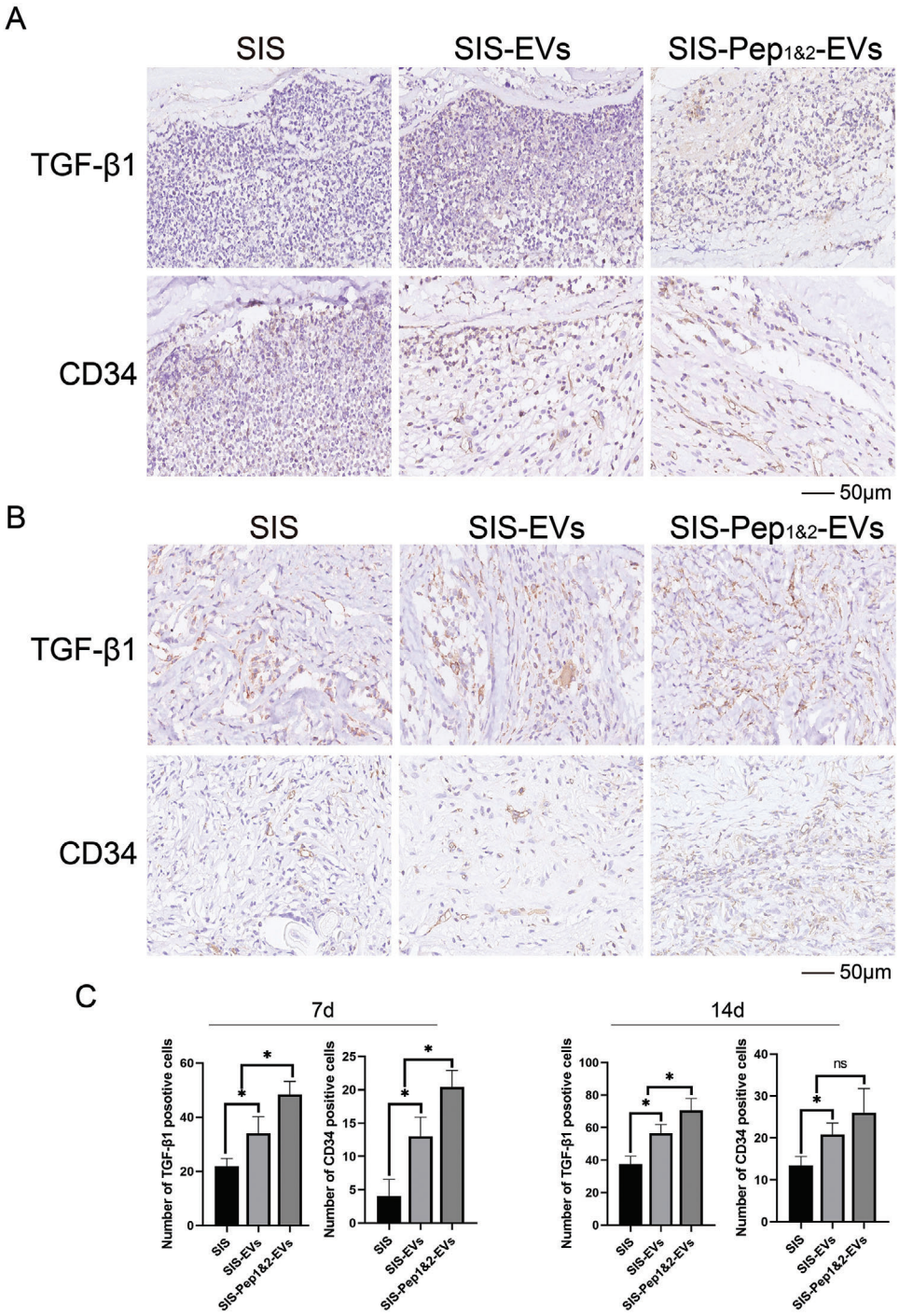

Figure 7. Representative immunohistochemical images of TGF-β1 and CD34 in the operating area of the SIS, SIS-EVs, and SIS-Pep$_{1\&2}$-EVs groups at A) 7 d and B) 14 d. C) Statistical analysis of TGF-β1 positive cells and CD34 positive cells. All data were displayed as mean ± SD, $n = 6$, $^*P < 0.05$. One-way ANOVA was used to analyze the results.

medium (DMEM) (Gibco, USA) supplemented with 10% EV-free FBS and 1% penicillin and streptomycin (Gibco, USA). Cells were cultured under condition of 5% CO_2 at 37 °C. After cells reached 80–85% confluency, the culture medium was replaced and collected and then preserved at −80 °C.

Isolation and Characterization of EVs: Preserved cell culture medium was centrifuged at 500*g* for 20 min, followed by centrifugation at 3000*g* for 20 min and 20 000*g* for 1 h at 4 °C. Then, the supernatant was collected and filtered through a 0.22-μm filter (Millex, USA) to remove cell debris and large cell vesicles. Subsequently, the samples were ultracentrifuged at 100 000*g* continuously for 4 h. The supernatant was discarded, and sterilized PBS was used to resuspend EVs. EVs were obtained by centrifugation at 100 000*g* for another 1 h. Finally, the obtained EVs were dissolved in

50 µL PBS and stored at −80 °C. The total protein concentration of EVs was quantified by the Pierce BCA Protein Assay Kit (Thermo Fisher Scientific, USA).

A nanoparticle size analyzer (Malvern, NS300, UK) was used to measure the size distribution of the EVs obtained. Morphology was visualized using a high-resolution TEM (Hitachi, HT7700, Japan). Finally, EVs were identified by western blot analysis using surface characteristic markers, including Alix, CD63, CD9, and the negative marker cytochrome C, with the corresponding antibodies (Abcam, UK).

Determination of Morphology and Size of EVs after Binding to Fusion Peptides: EVs were incubated with $Pep_{1\&2}$ and $Pep_{3\&4}$ overnight at 4 °C. Then TEM and NTA were used to examine the morphology and particle size.

Quantitative Relationship between Peptides and EVs: FITC-labeled $Pep_{1\&2}$ and $Pep_{3\&4}$ were co-incubated with 1 mg mL^{-1} EVs at 4 °C for 6 h, respectively. The unbound peptides were removed by diafiltration tube. Then, supernatant was detected by spectrophotometer. The standard curves were made to determine the concentration of fusion peptide. Particle concentration of EVs was obtained by NTA.

Preparation and Characterization of SIS Membranes Modified by Fusion Peptide-Mediated EVs: The SIS membranes used in this study were acellular porcine small intestinal submucosa obtained by decellularization and were generously provided by Bosis Healing Co., Ltd. (Beijing, China). Four fusion peptides were dissolved into 200×10^{-6} M peptide solution, respectively. And the same amount of peptide solution was used in the experiment. Pep1 and Pep2 were incubated with EVs at 4 °C for 6 h and transferred to 100 kD diafiltration tube (Millipore, USA) to remove a small amount of unbound peptides. The operation of Pep3 and Pep4 is the same as above. Subsequently, SIS membranes were cut into small pieces. One set of SIS membranes was only incubated with EVs, and the other two sets of SIS membranes were incubated with $Pep_{1\&2}$ solution and $Pep_{3\&4}$ solution both of which were added with EVs on a rotating mixer at 4 °C overnight. SIS membranes with EVs directly loaded were marked as SIS-EVs. SIS membranes combined with Peptide 1 and Peptide 2 were labeled SIS-$Pep_{1\&2}$-EVs, and those combined with Peptide 3 and Peptide 4 were labeled SIS-$Pep_{3\&4}$-EVs. The microstructure of modified SIS membranes was observed by SEM (ZEISS, Gemini 300, Germany). Before investigation, SIS membranes of different groups were freeze-dried and sprayed with gold.

Assays of the Fusion Peptide-Mediated EVs Binding to SIS: To detect the binding rate, samples were observed using a confocal laser scanning microscope (Carl Zeiss, LSM900, Germany) to obtain images. LHERHLNNN (collagen binding peptide I) was labeled with FITC (green), and KELNLVY (collagen binding peptide III) was labeled with Alexa Fluor 405 (blue). EVs were labeled with the DiI (red).

Loading Efficiency of Modified SIS Membranes: 200 µL EVs were incubated with fusion peptides to modify SIS membranes of each group, and these samples were incubated on a rotating mixer at 4 °C overnight. Then rinse twice with PBS. The supernatant of three groups was collected, and the content of EVs was detected by NTA to determine the loading efficiency.

Release of Fusion Peptides-Mediated EVs: Fluorescently labeled SIS-EVs, SIS-$Pep_{1\&2}$-EVs, and SIS-$Pep_{3\&4}$-EVs were immersed in PBS. After 1, 3, and 5 d, PBS was removed, and the cells were washed gently with PBS. The remaining fusion peptides and EVs were observed by CLSM.

Uptake of EVs by Cells: DiI-labeled EVs and the NIH3T3 cell line were cocultured. Cells were seeded in a 24-well plate (1×10^4 cells/well), and then EVs were added to the culture media and incubated for 12, 24, and 48 h. Cells were fixed with 4% paraformaldehyde (Solarbio, China) at room temperature for 10 min and permeabilized with 0.5% Triton X-100 for 10 min. Nuclei were stained with DAPI (Thermo Fisher Scientific, USA). Samples were visualized by CLSM.

Cell Viability Assay: NIH3T3 cells at passages 4–6 were used in this study. The viability of cells was measured by the CCK-8 assay. Briefly, after sterilization, SIS, SIS-EVs, SIS-$Pep_{1\&2}$-EVs, and SIS-$Pep_{3\&4}$-EVs samples were cut into circles with a diameter of 10 mm and placed into a 96-well plate. Subsequently, NIH3T3 cells were seeded in 96-well plates (2000, 100 µL/well). Three replicates were performed for each group. After 1, 2, 3, 4, 5, 6, and 7 d, 10 µL of CCK-8 reagent (Solarbio, China) was added to each well, followed by incubation for 2 h at 37 °C. OD value was calculated at 450 nm absorbance.

Migration and Cell Morphology Observation: To assess the migration ability of NIH3T3 cells, 1×10^4 cells/well were inoculated in the upper chamber of Transwell 24-well plates (Corning, NY) containing 5% EV-free FBS. Then, complete medium containing 10% FBS was added to the lower chamber supplemented with sterilized SIS, SIS-EVs, SIS-$Pep_{1\&2}$-EVs, and SIS-$Pep_{3\&4}$-EVs. After 24 h, Transwell chambers were removed and washed twice with PBS. The nonmigrated cells were gently wiped. Then, the cells were fixed with 4% paraformaldehyde for 30 min and stained with 0.1% crystal violet (Sigma-Aldrich, USA) for 30 min. Cells were washed three times with PBS. Cell migration images were observed with an optical microscope (Olympus, IX71, Japan).

To observe the cytoskeleton of cells in different groups, the membranes were seeded with NIH3T3 (1×10^4 cells/well). After 6 and 24 h of coculture, cells were fixed in 4% paraformaldehyde for 30 min and permeated in 0.5% Triton X-100 for 10 min. Cytoskeleton observation was obtained by Rhodamine B Phalloidin (Cytoskeleton, Inc., USA) staining. The nuclei were stained with DAPI. Cell morphology was observed by CLSM system. Mean cell area and perimeter were quantified using ImageJ software.

RNA-seq Assay: High-throughput sequencing was performed to detect the altered expression of miRNAs in different samples and enrichment pathways in tissue regeneration. NIH3T3 cells were seeded into six-well plates with SIS, SIS-EVs, SIS-$Pep_{1\&2}$-EVs, and SIS-$Pep_{3\&4}$-EVs. A blank plate without membrane was used as control. After 3 d, cells were scraped and collected and then sent to a company (Novogene Co., Ltd., Beijing, China) to carry out RNA-seq assays.

Quantitative Real-Time PCR: Collected cells were cultured in different groups. Total RNA was extracted by TRIzol Reagent (Invitrogen, USA). Synthesis of cDNA was completed using GoScript Reverse Transcription Mix (Promega, USA). Then, qRT-PCR analysis was performed with a LightCycler 480 II System (Roche, LC480 II, Switzerland). The mRNA expression changes of Vgll3, TEAD1, CYR61, and BIRC5 were detected quantitatively using the relative standard curve method ($2^{-\triangle\triangle CT}$). GAPDH was used as control. The PCR primer sequences used in this study are listed in Table S2 (Supporting Information).

Western Blot: Cells in each group were collected and lysed with RIPA (Solarbio, China) to extract protein. Protein from cultured cells was separated by sodium dodecyl sulfate-polyacrylamide gel electrophoresis (SDS-PAGE) and transferred to polyvinylidene fluoride membranes (Immobilon P, Millipore, Billerica, USA). After blocking with 5% bovine serum albumin (BSA, Sigma-Aldrich, USA) for 1 h at room temperature, the membranes were incubated with primary antibodies at 4 °C overnight, followed by incubation with horseradish peroxidase-conjugated secondary antibodies (Abcam, USA) at 37 °C for 1 h. Primary antibodies included antiYAP1, antiTEAD1, antiCYR61 and antiGAPDH antibodies (Abcam, USA). The final bands were visualized using ChemiDoc XRS Plus luminescent image analyzers (Bio-Rad, USA) after adding ECL Substrate (Thermo Fisher Scientific, USA). Densitometric quantification of band intensity was carried out with ImageJ software, and the relative expression level of the target protein was normalized to the band intensity of GAPDH.

Immunofluorescence Staining: After 3 d of culture, cells cultured in different groups were fixed with 4% paraformaldehyde, permeabilized with 0.5% Triton X-100, and sealed at room temperature. The cells were incubated overnight at 4 °C with a CYR61 primary antibody at a 1:200 dilution. Then, Alexa Fluor 488-conjugated antirabbit secondary antibody (Abcam, USA) was added to the samples and incubated at room temperature for 1 h. Nuclei were stained with DAPI. CLSM was used to obtain images.

Establishment and Repair of Abdominal Wall Defect Model in Rats: Male Sprague-Dawley (SD) rats aged 6–8 weeks (200–2250 g) were used in this study. The animal experiment was approved by the Animal Ethnic Committee of Tianjin Medical University. Rats were divided into three groups: SIS, SIS-EVs, and SIS-$Pep_{1\&2}$-EVs groups. Six replicates were used in each group. Rats were anesthetized with isoflurane through inhalation. After sterilization, round full-thickness defects with a diameter of 1 cm were made on the lateral wall of the abdomen. The defects were then repaired by fixing SIS, SIS-EVs, or SIS-$Pep_{1\&2}$-EVs. Then, the surgery area was sutured in layers.

In Vivo Toxicity Study: To determine the toxicity of the modified SIS membranes in vivo, blood was collected from the angular vein of rats and samples were placed in EP tubes. The serum was collected by centrifugation at 3000 rpm for 15 min. The levels of ALT, AST, BUN, and Crea were analyzed in the clinical laboratory (Tianjin Medical University Chu Hisen-I Memorial Hospital, Tianjin, China).

Morphological Observation and Pathological Analysis: For each group, animals were euthanized to collect implants and surrounding tissue at 7, 14, and 30 d after the operation. The morphology of tissues around the operation area was recorded. Samples were embedded in paraffin, dehydrated with ethanol, and then made into sections with a thickness of 5 µm. H&E staining and Masson trichrome staining (Solarbio, China) were carried out to evaluate tissue regeneration. The number of inflammatory cells and the percentage of collagen deposition were calculated by ImageJ.

For immunohistochemical analysis, sections were incubated overnight at 4 °C with primary antibodies against TGF-β1 and CD34 (Abcam, USA) at a 1:200 dilution. Then, the slices were incubated with the secondary antibody for 1 h at room temperature. Subsequently, the sections were incubated with DAB substrate to visualize antibody binding. After hematoxylin counterstaining, the images were observed by the whole landscape imaging quantitative analysis system (PerkinElmer, Vectra Polaris, USA). The number of TGF-β1 positive cells and CD34 positive cells was measured by ImageJ.

Statistical Methods: All results were statistically analyzed by SPSS v.21.0 software. One-way ANOVA was used to compare the mean values of the data. All data are expressed as mean ± standard deviations of at least three replicate experiments. A value of $P < 0.05$ was considered statistically significant ($^*p < 0.05$).

Supporting Information

Supporting Information is available from the Wiley Online Library or from the author.

Acknowledgements

L.Z., S.M., and Z.L. contributed equally to this work. This work was jointly supported by the National Natural Science Foundation of China (NSFC, Grant No. 81701019), the Scientific Foundation of Tianjin Education Commission (Grant No. 2019KJ173), the Science and Technology Project of Tianjin Health Committee (Grant No. QN20026), and the China Postdoctoral Science Foundation (Grant Nos. 2019M660270 and 2020M680253).

Conflict of Interest

The authors declare no conflict of interest.

Data Availability Statement

The data that support the findings of this study are available from the corresponding author upon reasonable request.

Keywords

extracellular vesicles, fusion peptide, microenvironments, small intestinal submucosa, tissue injury, tissue regeneration

Received: July 2, 2021
Revised: September 13, 2021
Published online:

[1] D. W. Song, S. H. Kim, H. H. Kim, K. H. Lee, C. S. Ki, Y. H. Park, *Acta Biomater.* **2016**, *39*, 146.
[2] a) M. Kelly, K. Macdougall, O. Olabisi, N. McGuire, *Int. Urogynecol. J.* **2017**, *28*, 171; b) U. Klinge, B. Klosterhalfen, A. P. Ottinger, K. Junge, V. Schumpelick, *Biomaterials* **2002**, *23*, 3487.
[3] B. Fan, Z. Wei, X. Yao, G. Shi, X. Cheng, X. Zhou, H. Zhou, G. Ning, X. Kong, S. Feng, *Cell Transplant.* **2018**, *27*, 853.
[4] B. Andree, A. Bar, A. Haverich, A. Hilfiker, *Tissue Eng., Part B-Re* **2013**, *19*, 279.
[5] a) Y. Ji, J. Zhou, T. Sun, K. Tang, Z. Xiong, Z. Ren, S. Yao, K. Chen, F. Yang, F. Zhu, X. Guo, *J. Biomed. Mater. Res., Part A* **2019**, *107*, 689; b) Z. L. Wang, S. Z. Wu, Z. F. Li, J. H. Guo, Y. Zhang, J. K. Pi, J. G. Hu, X. J. Yang, F. G. Huang, H. Q. Xie, *J. Biomater. Sci., Polym. Ed.* **2018**, *29*, 663.
[6] A. Hassanshahi, M. Hassanshahi, S. Khabbazi, Z. Hosseini-Khah, Y. Peymanfar, S. Ghalamkari, Y. W. Su, C. J. Xian, *J. Cell. Physiol.* **2019**, *234*, 7903.
[7] a) Y. Wang, X. D. Chen, W. Cao, Y. F. Shi, *Nat. Immunol.* **2014**, *15*, 1009; b) H. Li, X. Fu, *Cell Tissue Res.* **2012**, *348*, 371.
[8] P. R. Vulliet, M. Greeley, S. M. Halloran, K. A. MacDonald, M. D. Kittleson, *Lancet* **2004**, *363*, 783.
[9] a) D. G. Phinney, M. F. Pittenger, *Stem Cells* **2017**, *35*, 851; b) S. Rani, A. E. Ryan, M. D. Griffin, T. Ritter, *Mol. Ther.* **2015**, *23*, 812.
[10] a) G. Desdin-Mico, M. Mittelbrunn, *Cell Adhes. Migr.* **2017**, *11*, 127; b) A. Takahashi, R. Okada, K. Nagao, Y. Kawamata, A. Hanyu, S. Yoshimoto, M. Takasugi, S. Watanabe, M. T. Kanemaki, C. Obuse, E. Hara, *Nat. Commun.* **2017**, *8*, 15287; c) D. Karpman, A. Tontanahal, F. Radic, *Biol. Med.* **2021**, *171*, 42.
[11] A. Golchin, S. Hosseinzadeh, A. Ardeshirylajimi, *J. Cell. Biochem.* **2018**, *119*, 5043.
[12] a) P. P. Wu, B. Zhang, H. Shi, H. Qian, W. R. Xu, *Cytotherapy* **2018**, *20*, 291; b) J. Lelek, E. K. Zuba-Surma, *Int. J. Mol. Sci.* **2020**, *21*, 799.
[13] B. C. Yang, M. J. Kuang, J. Y. Kang, J. Zhao, J. X. Ma, X. L. Ma, *Biochem. Biophys. Res. Commun.* **2020**, *524*, 883.
[14] a) Y. Zhang, J. Xu, Y. Chai, J. Zhang, Z. Hu, H. Zhou, *Burns* **2019**, *45*, 950; b) W. Y. Li, Y. S. Liu, P. Zhang, Y. M. Tang, M. Zhou, W. R. Jiang, X. Zhang, G. Wu, Y. S. Zhou, *ACS Appl. Mater. Interfaces* **2018**, *10*, 5240.
[15] O. G. Chepurny, R. L. Bonaccorso, C. A. Leech, T. Wollert, G. M. Langford, F. Schwede, C. L. Roth, R. P. Doyle, G. G. Holz, *Sci. Rep.* **2018**, *8*, 3749.
[16] T. Kitajima, H. Terai, Y. Ito, *Biomaterials* **2007**, *28*, 1989.
[17] a) M. Horn, I. Neundorf, *Sci. Rep.* **2018**, *8*, 16279; b) C. Zhang, L. H. Liu, W. X. Qiu, Y. H. Zhang, W. Song, L. Zhang, S. B. Wang, X. Z. Zhang, *Small* **2018**, *14*, 1703321.
[18] a) X. Gao, N. Ran, X. Dong, B. Zuo, R. Yang, Q. Zhou, H. M. Moulton, Y. Seow, H. Yin, *Sci. Transl. Med.* **2018**, *10*, eaat0195; b) D. M. Pegtel, S. J. Gould, *Annu. Rev. Biochem.* **2019**, *88*, 487; c) E. J. K. Kowal, D. Ter-Ovanesyan, A. Regev, G. M. Church, *Methods Mol. Biol.* **2017**, *1660*, 143.
[19] a) R. Sistiabudi, A. Ivanisevic, *Langmuir* **2008**, *24*, 1591; b) C. E. Tye, G. K. Hunter, H. A. Goldberg, *J. Biol. Chem.* **2005**, *280*, 13487.
[20] X. Y. Chen, J. L. Zaro, W. C. Shen, *Adv. Drug Delivery Rev.* **2013**, *65*, 1357.
[21] D. Y. Wen, S. F. Foley, X. L. Hronowski, S. Gu, W. Meier, *Anal. Chem.* **2013**, *85*, 4805.
[22] J. M. Kovacs, C. T. Mant, R. S. Hodges, *Biopolymers* **2006**, *84*, 283.
[23] Y. Zhang, Y. Chen, B. Zhao, J. Gao, L. Xia, F. Xing, Y. Kong, Y. Li, G. Zhang, *Regener. Biomater.* **2020**, *7*, 577.
[24] a) J. Wang, *Protein Sci.* **2019**, *28*, 472; b) C. Castano, A. H. Thomas, C. Lorente, *Photochem. Photobiol.* **2021**, *97*, 91.
[25] H. Y. Chen, Z. Chen, B. G. Wu, J. Ullah, T. X. Zhang, J. R. Jia, H. C. Wang, T. W. Tan, *J. Mol. Microbiol. Biotechnol.* **2017**, *27*, 64.

[26] A. Casado-Diaz, J. M. Quesada-Gomez, G. Dorado, *Front. Bioeng. Biotechnol.* **2020**, *8*, 146.
[27] S. Horibe, T. Tanahashi, S. Kawauchi, Y. Murakami, Y. Rikitake, *BMC Cancer* **2018**, *18*, 47.
[28] P. D. Stahl, G. Raposo, *Physiology* **2019**, *34*, 169.
[29] K. C. Lin, T. Moroishi, Z. Meng, H. S. Jeong, S. W. Plouffe, Y. Sekido, J. Han, H. W. Park, K. L. Guan, *Nat. Cell Biol.* **2017**, *19*, 996.
[30] a) L. X. Chen, J. Ding, B. X. Wang, X. W. Chen, X. J. Ying, Z. W. Yu, P. Dong, *Exp. Cell Res.* **2021**, *404*, 112664; b) J. Tome-Garcia, P. Erfani, G. Nudelman, A. M. Tsankov, I. Katsyv, R. Tejero, B. Zhang, M. Walsh, R. H. Friedel, E. Zaslaysky, N. M. Tsankova, *Nat. Commun.* **2018**, *9*, 4020.
[31] J. A. McKenzie, T. Liu, A. G. Goodson, D. Grossman, *Cancer Res.* **2010**, *70*, 7927.
[32] Y. Wang, A. J. Yu, F. X. Yu, *Protein Cell* **2017**, *8*, 349.
[33] N. Figeac, A. D. Mohamed, C. Sun, M. Schonfelder, D. Matallanas, A. Garcia-Munoz, E. Missiaglia, E. Collie-Duguid, V. De Mello, A. V. Pobbati, J. Pruller, O. Jaka, S. D. R. Harridge, W. J. Hong, J. Shipley, N. Vargesson, P. S. Zammit, H. Wackerhage, *J. Cell Sci.* **2019**, *132*, jcs225946.
[34] a) Y. Hu, S. S. Rao, Z. X. Wang, J. Cao, Y. J. Tan, J. Luo, H. M. Li, W. S. Zhang, C. Y. Chen, H. Xie, *Theranostics* **2018**, *8*, 169; b) M. Alexander, R. Z. Hu, M. C. Runtsch, D. A. Kagele, T. L. Mosbruger, T. Tolmachova, M. C. Seabra, J. L. Round, D. M. Ward, R. M. O'Connell, *Nat. Commun.* **2015**, *6*, 7321.
[35] D. A. Dubay, W. Choi, M. G. Urbanchek, X. Wang, B. Adamson, R. G. Dennis, W. M. Kuzon, M. G. Franz, *Ann. Surg.* **2007**, *245*, 140.
[36] S. Barrientos, O. Stojadinovic, M. S. Golinko, H. Brem, M. Tomic-Canic, *Wound Repair Regener.* **2008**, *16*, 585.
[37] J. Qiao, Z. W. Jiang, Y. Yang, J. H. Chi, X. S. Qiao, B. Q. Han, W. S. Liu, *Carbohydr. Polym.* **2017**, *172*, 255.
[38] W. C. Chen, Y. K. Huang, J. C. Han, L. L. Yu, Y. L. Li, Z. Y. Lu, H. B. Li, Z. H. Liu, C. Y. Shi, F. Q. Duan, Y. Xiao, *Immunol. Res.* **2016**, *64*, 831.